Simultaneous local sensing of two chemical properties with dual Soft Probe Scanning Electrochemical Microscopy

- Supporting Information -

Gregorio Bonazza,[1] Hubert H. Girault,[2] Andreas Lesch*,[3] Salvatore Daniele* [1]

1) Department of Molecular Sciences and Nanosystems, Ca'Foscari University of Venice, 30123 Venice, Italy

2) Laboratory of Physical and Analytical Electrochemistry (LEPA), École Polytechnique Fédérale de Lausanne (EPFL) Valais Wallis, Rue del'Industrie 17, 1950 Sion, Switzerland

3) Department of Industrial Chemistry "Toso Montanari", University of Bologna, Viale del Risorgimento 4, 40136 Bologna, Italy

Corresponding author email addresses:
A.L.: andreas.lesch@unibo.it
S.D.: sig@unive.it

SI-1. Experimental details on Au electrode modification with IrO$_x$

The deposition solution was prepared by dissolving 0.4 mmol of K$_3$IrCl$_6$ in 25 mL of water and 0.5 mL of a 30% (w/w) H$_2$O$_2$ solution were then added for producing Ir(IV) species. After stirring for 30 minutes, 5.5 mM of C$_2$H$_2$O$_4$ were added for the formation of the [Ir(COO)$_2$(OH)$_4$]$_2$ complex. The solution was then made basic to pH 10.5 using K$_2$CO$_3$. The solution color changed from pale yellow to blue after four days indicating the complex formation. The first electrodeposition step was then carried out by applying a potential of 0.8 V *vs.* Ag/AgCl (sat. KCl) for 600 s, forming potentially IrO$_x$. In the second electrodeposition step, the IrO$_x$-coated gold microelectrode (ME) was cycled consecutively for at least five cycles over the potential window from 0 to 0.8 V at 100 mV/s either to increase the amount of IrO$_x$ deposited or to form the mixed Ir(IV)/Ir(III) oxides system. This procedure resulted to be effective to provide suitable stability to the IrO$_x$ layer. A procedure involving only use of a large numbers of CVs provided, in general, less stability of the IrO$_x$ layer.

SI-2. Diagnostic analysis of the CVs

The voltammetric parameters, steady-state limiting current (I_{exp}) and Tomes parameter ($E_{3/4} - E_{1/4}$) for the various dual soft probes are summarized in Table S2 [1]. Theoretical values, expected for diffusion limiting currents at an inlaid microdisc embedded in an infinite insulating plane (I_{the}), which can be predicted by Eq. S1 [2], are also included.

$$I_{theo} = 4 \cdot n \cdot F \cdot D \cdot c_{bulk} \cdot a \qquad\qquad\qquad\qquad (Eq. \ S1)$$

where n is the number of electrons transferred in the oxidation or reduction reaction, F is the Faraday constant, D is the diffusion coefficient of the electroactive species, c_{bulk} is the bulk concentration and a is the radius of the microdisc. Steady state voltammograms were recorded in a solution containing 1 mM FcMeOH ($D = 7.8 \times 10^{-6}$ cm^2 s^{-1} [3]) and 0.1 M KNO$_3$ as supporting electrolyte.

From Table S2 it is evident that, in general, experimental current values are larger than expected. This is due to the thin insulation sheath around half the microdisc geometry, which induces diffusion from behind the plane of the electrode, thus enhancing the flux (and consequently the current) to the inlaid disc [4, 5]. Instead, the Tomes parameter, for all the investigated soft probes, compares well with 56.3 mV, theoretical value expected for a reversible one-electron process at 25°C for either thin or thick insulating sheaths [4]. Theoretical equations predicting steady-state limiting normalized currents for thin shielded microelectrodes (I_{ssTF}) are available in the literature [4, 5]. However, they refer to symmetric insulating insulation layers surrounding the microelectrodes [4, 5], conditions that do not apply for the microdiscs of the soft probes developed here, where the thicknesses of the insulating sheaths are asymmetric. In fact, while the lateral insulating layer, th_L (Fig. 3b in the main text) is relatively thin (*i.e.*, varying from about 4 to 7 µm), the insulation layer of the main soft probe body from the other side, comprising dielectric layer and PET foil, is much ticker (i.e., > 180 µm). The following approximate analytical equation has been derived by interpolating simulated data, obtained to account for I_{ssTF} of microdiscs, surrounded by a uniform insulating sheath [5]:

$$I_{ssTF} = 1.000 + 0.1445 \ (RG - 0.6734)^{-0.8348} \qquad\qquad (Eq. \ S2)$$

where RG is the ratio of overall radius of the SECM tip (including insulator and microdisc) to the radius of the microdisc a. On the basis of Eq. S2, only the portion of the microdisc, i.e., the part that is embedded in the dielectric layer, opposite to the PET foil, is subjected to diffusion from behind the plane of the electrodes. Instead, diffusion from behind is negligible for the other side, being $RG > 10$ [4, 5]. Experimental steady-state currents shown in Table S2 suggest that the effect of the thin insulating shield over the entire microdisc surface is no more than about 9%. It must be considered

that if the above very thin insulating shields were uniform around the microdiscs, the steady-state currents would have deviated from those predicted by (Eq. S1) by about 20% and 16%, respectively.

Table S2. Steady-state plateau currents of CVs recorded at soft SECM probes with different thicknesses of dielectric material and different electrode materials. Pt and Au electrodes had a radius of 12.5 μm, the C electrode 4 μm.

Electrode material	$th_{dielectric}$ (μm)	I_{the} (nA) [1]	I_{exp} (nA)[2]	I_{exp}/I_{the}	$(E_{3/4} - E_{1/4})$[3](mV)
Pt	27	3.76	4.11	1.09	59
Au	27	3.76	4.05	1.08	58
C	27	1.12	1.22	1.09	61
Pt	29	3.76	3.88	1.03	57
Au	29	3.76	3.97	1.06	58
C	29	1.12	1.13	1.01	59
Pt	35	3.76	3.85	1.02	60
Au	35	3.76	3.68	0.98	59
C	35	1.12	1.09	0.97	62

(1) Theoretical (the) current expected for an inlaid disk microdisc with infinitely wide insulating sheath

(2) Experimental values.

(3) Experimental Tomes parameter. Theoretical value at 25 °C = 56 mV.

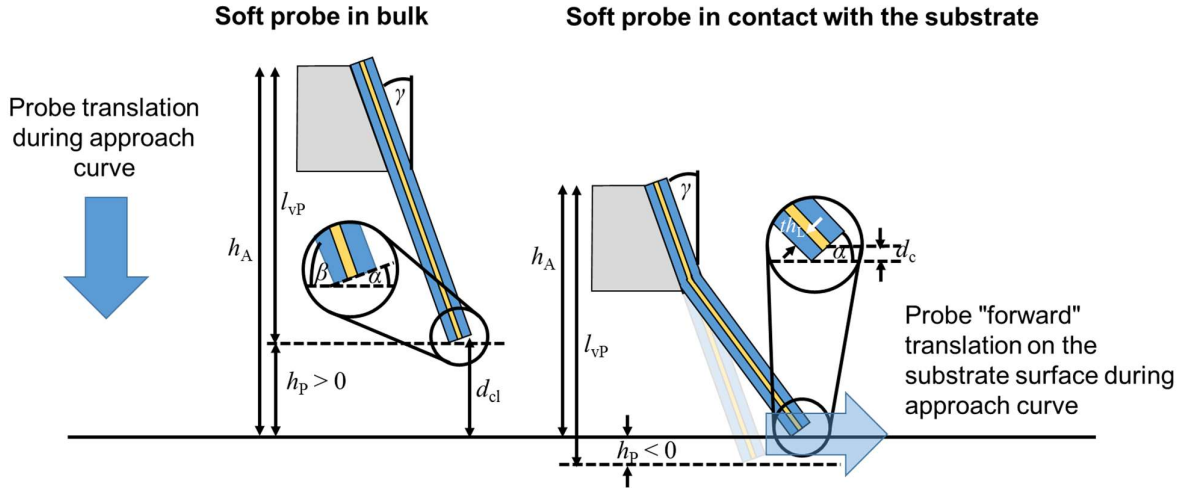**SI-3. Explanations on soft probe translations and its geometric parameters**

Fig. S3-1. Schematic representation of the mounting of the soft probe to the probe holder connected to the *z*-axis during vertical probe approaching at two locations: in the solution bulk (left) and when already in contact with the substrate (right).

The soft probe was placed in a custom-made probe holder with an inclination angle of $\gamma = 20°$ with respect to the surface normal of the substrate. The vertical length l_{vP} of the soft probe and the vertical height of the attachment point of the soft probe above the substrate surface (h_A) are geometric considerations of interest. While l_{vP} is a constant h_A changes with distance of the probe holder to the substrate surface. The vertical difference between h_A and l_{vP} defines the height of the probe h_P:

$$h_P = h_A - l_{vP} \tag{Eq. S2}$$

As a consequence, h_P has positive values when the soft probe does not contact the substrate and has negative values when it touches the substrate. Therefore, during an approach curve h_P becomes negative after the tip of the soft probe touched the substrate surface and is approached further against the substrate. The angle α describes the geometric arrangement of the probe cross-section, which includes the active area of the microelectrode, and the substrate surface. As described in the main manuscript, th_L represents the thickness of the dielectric ink between the electrode wire and surface of the dielectric material. With these geometric parameters, the effective working distance d between the tilted soft probe and the horizontally oriented substrate surface can be calculated for two distinct cases, which are i.) the soft probe being freely suspended in the solution bulk ("contact-less") or ii.) the soft probe being in contact with the substrate ("contact").

$$\text{contact-less: } d_{cl} = h_P + th_L \cdot \sin \alpha; \ h_P > 0 \qquad \text{(Eq. S3)}$$

$$\text{contact: } \quad d_c = th_L \cdot \sin \alpha; \ h_P \le 0 \qquad \text{(Eq. S4)}$$

However, the working distance of the soft probe for SECM imaging is in daily praxis of less importance than h_P, as the working distance depends on the probe angle (that can be flexibly changed by the operator), and the angle of the cut cross-section, creating the necessity to calculate the working distance for each situation based on microscopic inspections. h_P instead is a parameter directly accessible from approach curves.

Soft probe translation over the substrate surface with the tip of the soft probe being in contact with the substrate
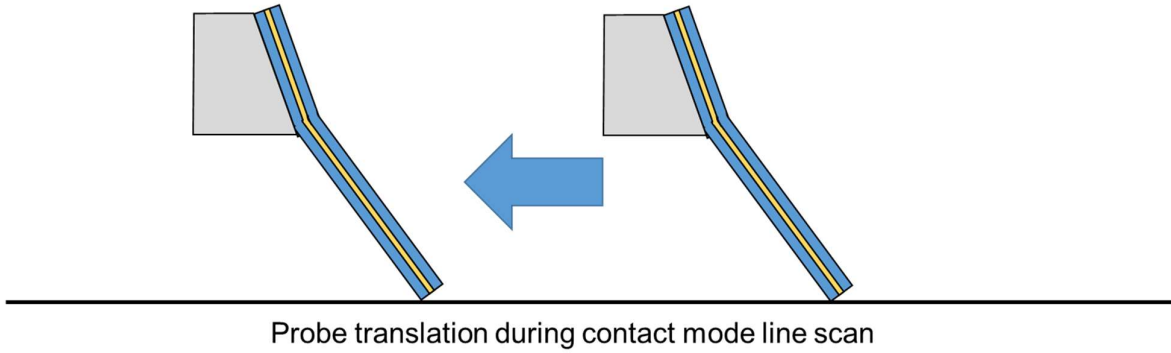

Probe translation during contact mode line scan

Fig. S3-2. Schematic representation of the translation of the soft probe during SECM line scans and imaging.

SI-4. Characterization of the soft platinum black (PtB)-modified Pt microdisc electrode

Geometric electrode areas A_{geo} of Pt and PtB/Pt electrodes were determined before and after the electrodeposition of PtB by recording the plateau currents of the steady-state CVs in a solution containing 1 mM FcMeOH, and 0.1 M KNO$_3$ to calculate the microdisc radii. Fig S4a shows typical CVs obtained with a soft PtB/Pt (red curve) and a bare Soft Pt ME (black curve). The electrochemically active surface area A_{real} of the PtB/Pt microelectrode was determined by cyclic voltammetry in 0.5 M H$_2$SO$_4$ using the currents in the region of hydrogen UPD process [6, 7]. Fig S4b shows typical cyclic voltammograms obtained at 200 mVs^{-1} over the potential range -0.3 – -0.7 V vs Pt pseudo-reference electrode (Pt-PRE) with a PtB/Pt (red curve in Fig S4b) and that of the corresponding bare Pt microelectrode before platinum black deposition (black line in Fig S4b). As it can be seen, for both microelectrodes the typical voltammetric features for polycrystalline Pt are observed.

The larger current involved at the PtB/Pt microelectrode compared to that of the Pt microelectrode is clearly due to the enhanced effective electrochemical surface area. From the charge involved in the hydrogen adsorption/desorption in process over the potential range between -0.4 and -0.7 V vs Pt-PRE, after subtraction of the double layer charge and assuming a monolayer of hydrogen corresponding to an adsorption of 210 μC/cm^2 [8], the A_{real} of the PtB/Pt microelectrode and bare Pt microelectrode were determined given thereafter the roughness factors $RF = A_{real}/A_{geo}$ of 28.2 and 3.1, respectively.
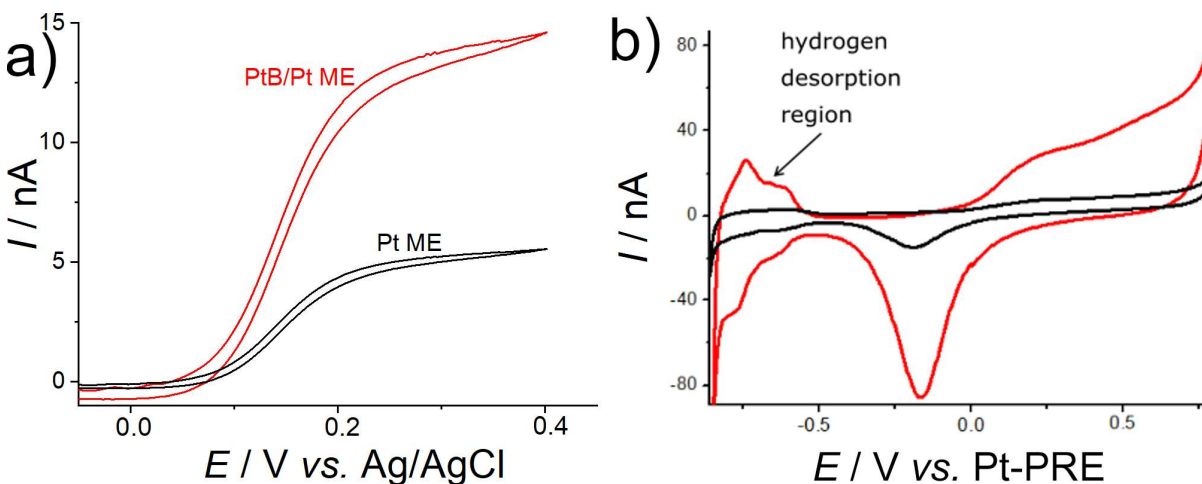

Fig S4. a) CV recorded at a 25 μm soft Pt ME in 1 mM FcMeOH in 0.1 M KNO$_3$ before (black line) and after (red line) platinum black deposition. Scan rate: 20 mV/s. a) CV (15 cycles) recorded at Pt microelectrode in 0.5 M H$_2$SO$_4$ before (black line) and after (red line) platinum black deposition. Potential scan rate 200 mV/s.

SI-5. Fabrication and characterization of soft IrO$_x$/Au

The electrodeposition of thin layer films of IrO$_x$ onto the soft Au microelectrode was carried out as described SI-1. The first step involved the electrodeposition of an IrO$_2$ film at constant potential of 0.8 V vs. Ag/AgCl (sat. KCl) for 600 s (Fig S5a) following the overall reaction described in Eq. S4 [9].
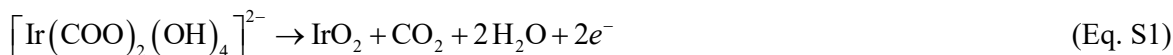
$$\left[Ir(COO)_2(OH)_4 \right]^{2-} \rightarrow IrO_2 + CO_2 + 2H_2O + 2e^-$$ (Eq. S1)

Fig S5b shows CVs recorded with the soft IrO$_x$/Au ME in phosphate buffered solution (pH 7, black curve) and in H$_3$PO$_4$ at pH 1.9. The typical anodic peak corresponding to the oxidation of Ir(III) to Ir(IV) and cathodic peak for the reduction of Ir(IV) to Ir(III) can be seen [10]. Both peak potentials are nearly overlapping as known for a surface-confined redox species.
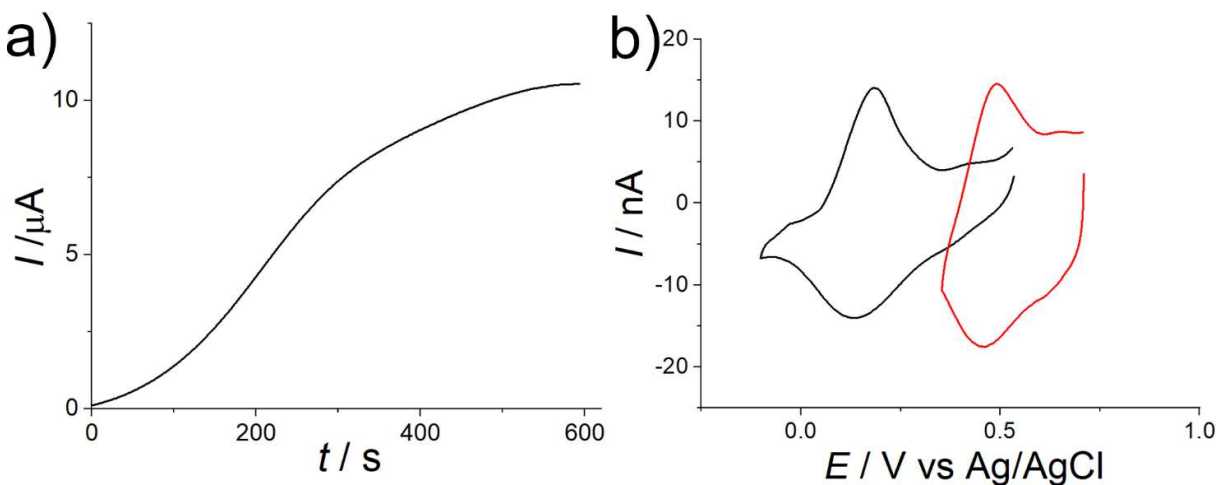

Fig S5. a) Electrochemical deposition of IrO$_2$ on a soft Au ME by applying a constant E_T of +0.8 V vs. Ag/AgCl in the deposition solution. b) CVs of a soft IrO$_x$/Au ME recorded in phosphate buffered solution (pH 7, black curve) and in phosphoric acid of pH 1.9 (red curve). Potential scan rate 50 mV/s.

SI-6. Characterization of pH microsensor

The dependence of the IrOx prepared here was preliminary assessed by measuring potential values at open circuit (E) in 0.1 mol L^{-1} $HPO_4^{2-}/H_2PO_4^-$ solutions at different pH values in the range 3 to 7, adjusted by addition of HNO_3 or NaOH solutions. E responses obtained as a function of time are shown in Fig S6a with a representative inset showing the response time of the IrO_x-Au microelectrodes to pH changes. The E at the IrO_x/Au changed with pH resulting in a slope of -61 mV/pH (Fig. S6b).
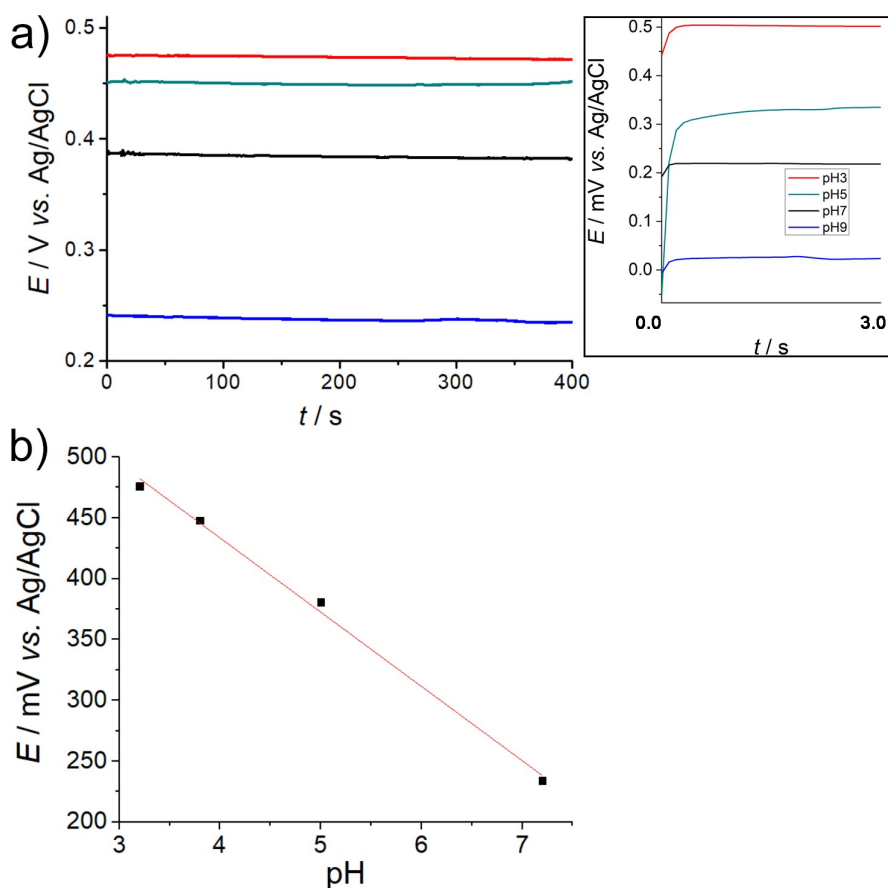

Fig. S6. Potentiometric use of a soft IrO_x-Au SECM probe for pH sensing. a) E *vs* time recorded at different HNO_3 concentrations (from 0 to 5×10^{-4} M) in 0.1 M KNO_3 solutions. Inset shows the soft pH probe response time (at short times) of an identically prepared IrO_x-Au microelectrode in solutions of different pH values, i.e., 3,5,7 and 9. b) E *vs.* pH diagram of the values (from the main figure in a)).

The calibration plot and the buffer solutions were also used to check the stability of the IrO_x/Au microelectrode of the soft dual probe and the reliability of the data obtained after performing series of SECM measurements. In case of anomalous behaviors, the IrO_x layer was renewed. For instance, a possible inconsistency was the observation that the current at the PtB/Pt increased (indicating the

formation of RNS and the consequent consumption of H^+), while the pH measured with IrO_x/Au decreased. This is opposite of what is expected on the basis of reactions (2)-(7) shown in the main text.

SI-7 Effect of probe translation rate on SECM line scan response

In order to analyze the effect of the probe translation speed on the evaluation of the RNS, line scans were recorded above a Ag microband immersed in 0.2 mM HNO_3 using also slower scan rates than 20 μm/s (Fig. S7). The maximum currents for all measurements correspond to each other demonstrating that 20 μm/s can be used for contact mode SECM scanning with the soft probes presented herein.
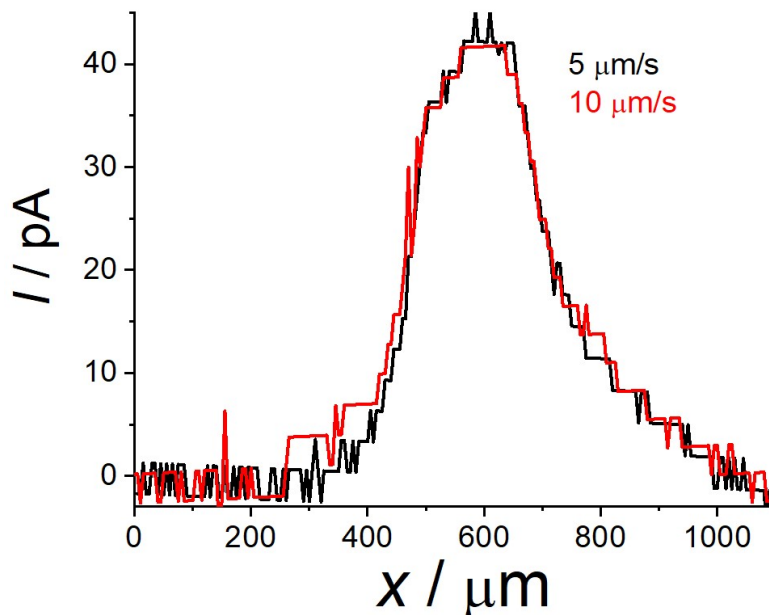

Fig. S7. Current (I) profiles as a function of the scanned distance in x direction (baseline-corrected), due to RNS, recorded with PtB/Pt microelectrode of the soft probe at different translation speeds as indicated in the figure. Applied potential at the PtB/Pt microelectrode of 0.8 V vs. Ag/AgCl.

SI-8. Control SECM line scan under neutral conditions

Control experiments were performed with the Ag band immersed in the neutral 0.1 M KNO₃ electrolyte, where corrosion of Ag should be negligible or would proceed to a much slower extent. Fig. S8 shows current and E changes observed under the latter conditions, while the soft probe was linearly scanned on the Ag surface.
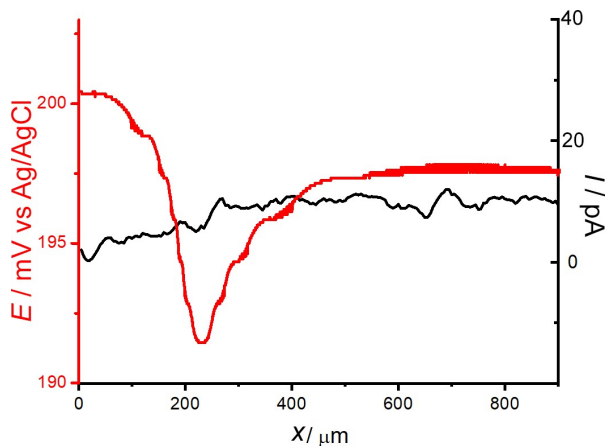

Fig. S8. Potentiometric (red) and amperometric (black, baseline-corrected) responses recorded performing a line scan over Ag pattern at the soft dual IrO$_x$/Au – PtB/Pt Probe in 0.1 M KNO₃. E measurement at IrO$_x$/Au soft probe, E_P = 0.8 V at PtB/Pt soft probe for RNS detection. Probe translation speed 5 µm/s.

References

[1] A.M. Bond, K.B. Oldham, C.G. Zoski, Steady-state voltammetry, Anal. Chim. Acta, 216 (1989) 177-230.

[2] Y. Saito, A theoretical study on the diffusion current at the stationary electrodes of circular and narrow band types, Rev. Polarogr. , 15 (1968) 177-187.

[3] W. Miao, Z. Ding, A.J. Bard, Solution viscosity effects on the heterogeneous electron transfer kinetics of ferrocenemethanol in dimethyl sulfoxide-water mixtures, J. Phys. Chem. B, 106 (2002) 1392-1398.

[4] I. Ciani, S. Daniele, Voltammetric determination of the geometrical parameters of inlaid microdisks with shields of thickness comparable to the electrode radius, Anal. Chem., 76 (2004) 6575-6581.

[5] S. Daniele, I. Ciani, D. Battistel, Effect of the insulating shield thickness on the steady-state diffusion-limiting current of sphere cap microelectrodes, Anal. Chem., 80 (2008) 253-259.

[6] A. Kicela, S. Daniele, Platinum black coated microdisk electrodes for the determination of high concentrations of hydrogen peroxide in phosphate buffer solutions, Talanta, 68 (2006) 1632-1639.

[7] S. Trasatti, O.A. Petrii, International Union of Pure and Applied Chemistry Physical Chemistry Division Commission on Electrochemistry: Real Surface Area Measurements in Electrochemistry, Pure Appl. Chem., 63 (1991) 711-734.

[8] W.H. Reinmuth, Three-Dimensional Representation of Voltammetric Processes, Anal. Chem., 32 (1960) 1509-1512.

[9] E. Bitziou, D. O'Hare, B.A. Patel, Simultaneous detection of pH changes and histamine release from oxyntic glands in isolated stomach, Anal. Chem., 80 (2008) 8733-8740.

[10] I.G. Casella, M. Contursi, R. Toniolo, Anodic electrodeposition of iridium oxide particles on glassy carbon surfaces and their electrochemical/SEM/XPS characterization, J. Electroanal. Chem., 736 (2015) 147-152.